RSC Advances

ROYAL SOCIETY OF CHEMISTRY

www.rsc.org/advances

RSC Advances

ARTICLE

Structure and electrochemical detection of xenobiotic micro-pollutant hydroquinone using CeO_2 nanocrystals

Received 00th January 20xx,
Accepted 00th January 20xx

DOI: 10.1039/x0xx00000x

www.rsc.org/

N. Sabari Arul,[a,*] D. Mangalaraj,[b] Jeong In Han,[a,*] and L.S. Cavalcante,[c]

In this study, cerium oxide nanocrystals (CeO_2 NCs) were synthesized by the simple and cost effective precipitation method. The structural properties of the obtained CeO_2 NCs were characterized by means of X-ray diffraction (XRD) with Rietveld refinement analysis, Transmission electron microscopy (TEM). X-ray photoelectron spectroscopy (XPS) and energy dispersive X-ray spectroscopy (EDX) confirms the presence of CeO_2 NCs. The structural properties confirmed the presence of cubic fluorite-type cubic structure which is in agreement with the respective Inorganic Crystal Structure Database (ICSD) N°. 156250. The hydroquinone (HQ) sensing of CeO_2 NCs/carbon paper (CP) modified electrode in 0.1 M phosphate buffer solution (pH=7) was characterized using a cyclic voltammetric (CV) electrochemical technique. The CV curve exhibited redox peaks with a detection limit of 0.111 mM and the linear ranges (0.03-0.8 mM) with a sensitivity of 2.443 mA mM^{-1} cm^{-2} for HQ detection. Our results indicate that CeO_2 NCs modified on CP holds as a promising candidate for the electrochemical detection of toxic HQ.

1. Introduction

Hydroquinone (HQ) is an isomer of dihydroxybenzene compounds which is considered a potential carcinogen candidate and xenobiotic micro-pollutant.[1] HQ is one of the highly toxic polluting chemical usually coexist in the environmental samples and get absorbed through skin and cause critical damage to the living beings.[2] United States environmental protection agency and European Union has listed HQ as the main pollutant to be monitored.[3] Moreover, this issues becomes highly fascinating to detect and quantify the leakage of HQ to avoid harmful effects on human health. Several methods were employed for the determination of chemical pollutants such as liquid chromatography, fluorescence, chemiluminescence, and spectrophotometry methods.[4-7] Although these techniques offers high sensitivity, they suffer from many drawbacks such as expensive equipment, extended period of sample preparations, complication in sample analysis etc.[8] In contrast, electrochemical methods show the advantages of short response time, environmental friendly, high sensitivity, cost effective, and high selectivity towards the analyte.[9] Recently, highly stable novel sensing materials with excellent conductivity including Pt nanoparticle decorated ZrO_2-RGO modified electrode,[10] Graphene-gold nanocomposite,[11] Graphene oxide/MnO_2 nanocomposites,[12] Polyaniline/Fe_2O_3/rGO,[13] Carbon nanocages/rGO composites,[14] Graphene/TiO_2,[15] WS_2-graphene,[16] and MnO_2/polyaniline[17] have been extensively investigated for the determination of HQ in the literature.

Cerium oxide (CeO_2) nanocrystals (NCs) is an important rare-earth oxide with fluorite type cubic structure and exhibit unique properties including improved redox properties, surface to volume ratio, oxygen defects that arises from electronic confinement of 4*f* orbitals.[18, 19] Recently, CeO_2 NCs has mesmerized significant interest of scientific society because of its wide band gap (3.2 eV) and considered as a promising materials for various application including photocatalyst, fuel cells, sensors, solar cells, electrochemical redox behaviours and biomedical applications.[20-26] In particular, CeO_2 NCs has been proved to be a highly sensitive electrode material in determining various toxic and hazardous gases and chemicals.[27-30] Even though several CeO_2 nanostructures have been extensively investigated in the development of non-enzymatic electrochemical sensors, to best of our knowledge, there is no report on the structural and electrochemical detection of hydroquinone using CeO_2 NCs.

Therefore, in this paper, we report the data for the chemical synthesis of CeO_2 NCs using precipitation method and their investigation on the electrochemical detection of HQ. Precipitation method is simple, cost effectiveness, high yield of products with purity.[31,32] The nanocrystals obtained were systematically characterized by means of X-ray diffraction (XRD), with Rietveld refinement analysis, X-ray photoelectron spectroscopy (XPS), energy dispersive X-ray spectroscopy (EDX) and Transmission electron microscopy (TEM). The electrochemical sensing of CeO_2 NCs modified electrodes exhibit good sensing behaviour towards the detection of HQ.

2. Experimental details

2.1. Synthesis of CeO_2 NCs

[a] Department of Chemical and Biochemical Engineering, Dongguk University–Seoul, 100715, South Korea. E-mail: artsabari@gmail.com, hanji@dongguk.edu Phone: +82 2 2290 1646, +82 2 2260 3364 Fax: 82 2 2268 8729.
[b] Department of Nanoscience and Technology, Bharathiar University, Coimbatore, 641046, India.
[c] CCN-PPGQ-DQ-GERATEC, Universidade Estadual do Piauí, João Cabral, N. 2231, P.O. Box 381, CEP: 64002-150 Teresina, PI, Brazil.

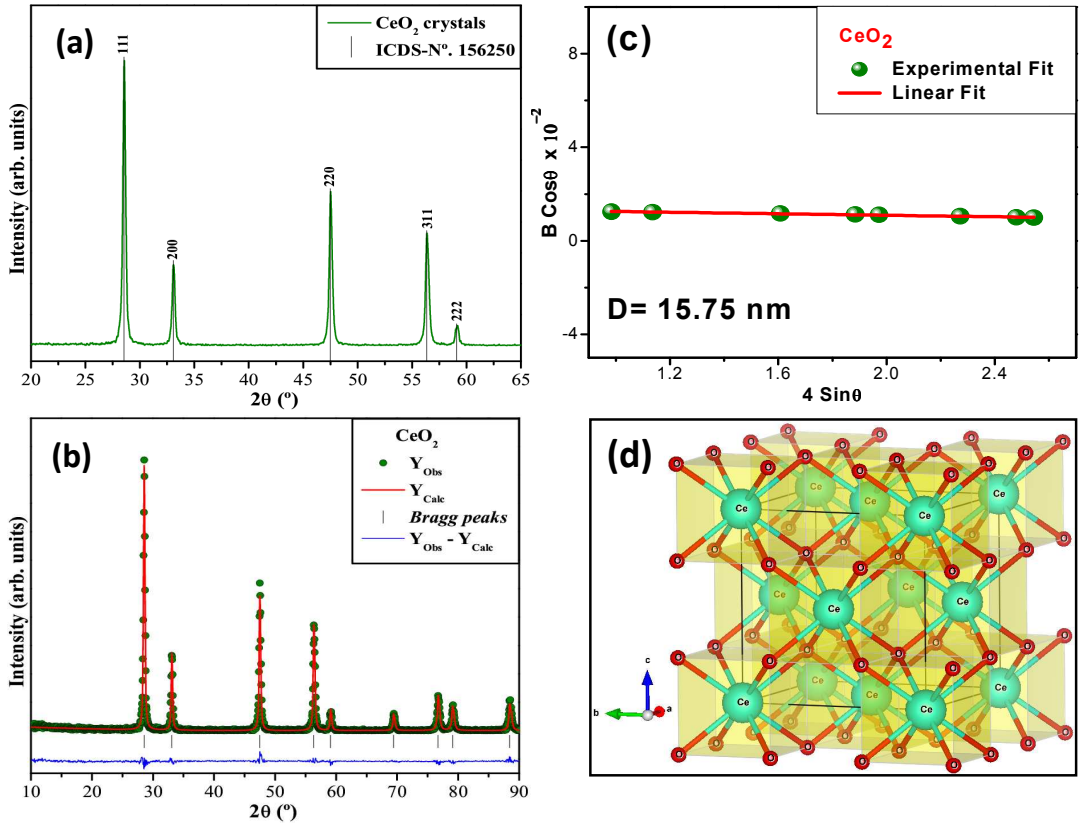

Fig. 1 (a) XRD patterns of CeO_2 nanocrystals with vertical dashed lines indicating the position and relative intensity of the respective ICSD Card N°. 156250 (b) Rietveld refinement plot, (c) W-H plot of synthesized CeO_2 nanocrystals (d) Schematic representation of a crystalline CeO_2 (1×1×1) unit cell which illustrates [CeO_8] clusters.

All chemical reagents used in the experiments were of analytical grade. Initially, 0.5 M of cerium (III) nitrate hexahydrate [$Ce(NO_3)_3.6H_2O$] was mixed in 20 ml of double distilled water and then precipitated by ammonium hydroxide (NH_4OH) solution (pH~10) under constant stirring at room temperature. The resultant colloidal solution was sealed in a beaker and aged for two days. The resultant precipitates were separated by centrifuging at 6000 rpm and washed several times with de-ionized water and ethanol to remove the impurities. The precipitate was dried in vacuum oven at 90° C for overnight to obtain CeO_2 NCs and then subjected further for characterization.

2.2 Characterizations

The crystal structure of the CeO_2 NCs was determined by using RIGAKU XRD/MAX-2200 diffractometer with Cu–Kα1 radiation (λ = 0.15418 nm). Transmission electron microscopy (TEM) was performed by using JEOL JEM-2100F system at an accelerating voltage of 200 kV. EDAX spectrum was obtained from FEI QUANTA-200 system operated at 30 kV. X-ray photoelectron microscopy (XPS) was performed using XPS-Kratos analytical instrument, ESCA-3400, Shimadzu with an X-ray source Mg Kα, and 1253.6 eV operated at 10 kV. The electrochemical measurements was performed using PCE200 Gamry frame work electrochemical workstation using a three electrode system in phosphate buffer solution (PBS, pH=7) as the electrolyte solution under ambient conditions. CeO_2 NCs supported on the carbon paper, a platinum wire, and Ag/AgCl was utilized as the working electrode, counter and electrode, respectively. The cyclic voltammetry (CV) measurements were performed at various scan rates in the potential range from -0.4 to 0.6 V. The modified working electrode was prepared as follows: Initially, a required amount of CeO_2 NCs was dispersed in 5 wt% of nafion and methanol (1:2) to obtain colloidal sol and the sol was coated on carbon paper containing an area and thickness of 1 x 1 cm and 0.02 cm, respectively. The modified electrode was dried at room temperature and subjected further for CV analysis.

3. Results and Discussion

X-ray diffraction pattern of the synthesized CeO_2 NCs is shown in Fig. 1(a). The results reveal that the synthesized sample has the cubic fluorite structure of CeO_2, which is consistent with the JCPDS card (#34-0394). In order to obtain precise structural insights of CeO_2 NCs, Rietveld refinement was carried out.[33] All XRD peaks corresponds to a cubic fluorite structure which is in agreement with the respective Inorganic Crystal Structure Database (ICSD) N°. 156250.[34] The Rietveld method is based on the construction of

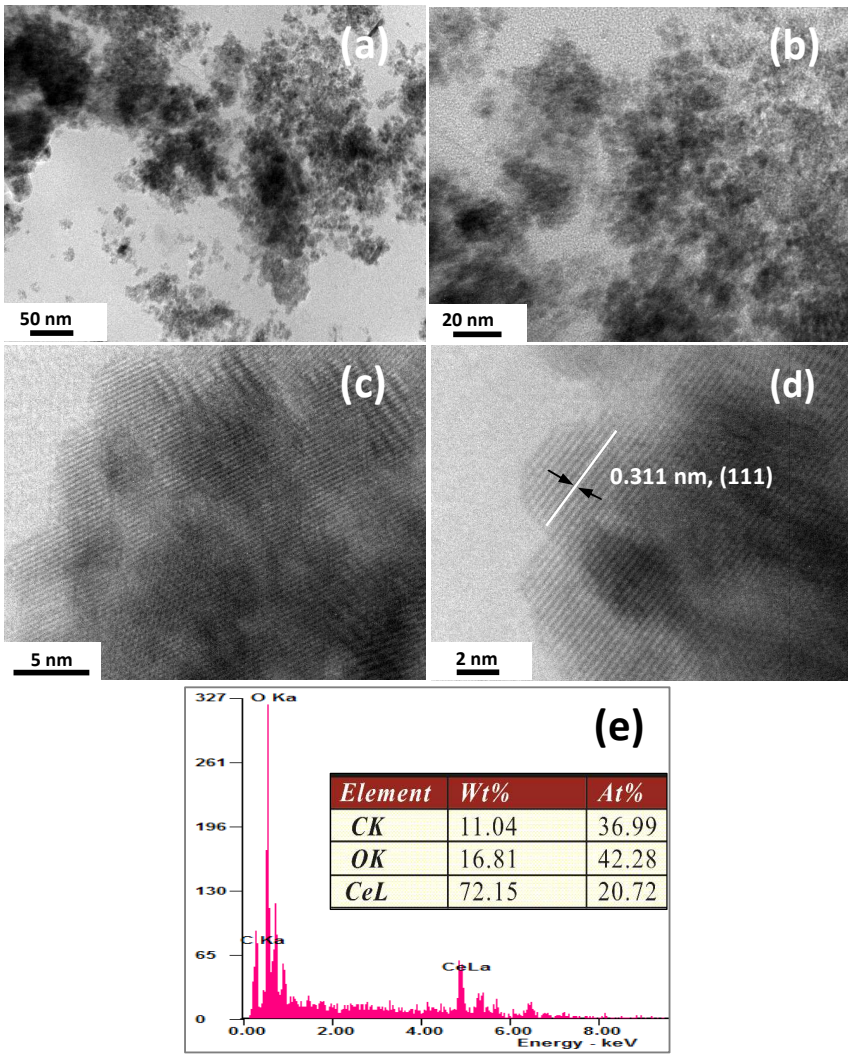

Fig. 2 (a-c) TEM images in different magnifications (d) HRTEM image (e) EDX spectrum of CeO_2 nanocrystals.

diffraction peak diffraction patterns calculated according to the structural model.[35,36] The points are the observed intensities and the line is the Rietveld fit, as shown in Fig. 1b. The Rietveld refinement was performed using the ReX V0.7.2 Powder diffraction program.[37] The background was corrected using Chebyschev polynomial of the first kind and the diffraction peak profiles were fitted by the Thompson–Cox–Hastings pseudo-Voigt (pV-TCH) function.[38] The obtained Rietveld parameters are listed in the Table. 1.

Table 1. Lattice parameters, unit cell volume, and atomic positions for CeO_2 Nanocrystals.

Atoms	Wyckoff	Site	x	Y	z	Occupancy	U_{iso}
Ce	4*a*	m-3m	0	0	0	1	0.00127
O	8*c*	-43m	0.25	0.25	0.25	1	0.02533

$Fm\bar{3}m$ (225) – Cubic (a=b=c = 5.411 Å; c/a = 1, V = 158.48 Å^3; Z=4); R_p = 10.4; R_{wp} = 6.5; R_{exp} = 5.6 and GoF =1.16.

The Rietveld refinement results indicate good agreement was obtained between the experimental relative intensities and the simulated intensities (Fig. 1b). Moreover, the difference between XRD patterns of experimental and calculated datas display small differences in the scale of intensity as illustrated by a line ($Y_{Obs} - Y_{Calc}$). The calculated lattice constants of the synthesized CeO_2 NCs are found to be 5.411 Å, which is consistent with that of bulk CeO_2 (5.416 Å).[39]

The crystallite size of CeO_2 NCs is estimated using Willamson-Hall (W-H) plot (Fig. 1c) using the obtained XRD pattern where the correction for peak broadening (B) is given by eq. (1),[40]

$$B^2 = (\beta^2_{experimental} - \beta^2_{intrumental}) \quad (1)$$

where $\beta^2_{experimental}$ is the integral breadth of each peak and $\beta^2_{intrumental}$ is the instrumental broadening determined from polycrystalline silicon standard.

The Williamson-Hall (W-H) equation is given as,

$$B\cos\theta = K\lambda/D + 4\varepsilon \sin\theta \quad (2)$$

where D is the crystallite size; K is the shape factor (0.9); λ is the wavelength of X-Ray source (1.54 Å), B is the integral width (in rad) estimated from eq. (1), θ is the angle of reflection (in deg) and ε is the inhomogeneous internal strain (in %). Fig. 1(c) shows the W-H plot for the synthesized CeO_2 crystals where the crystallite size calculated to be 15 nm (±0.5 nm) and it was observed that no heterogenous strains exisits in CeO_2 NCs.[31]

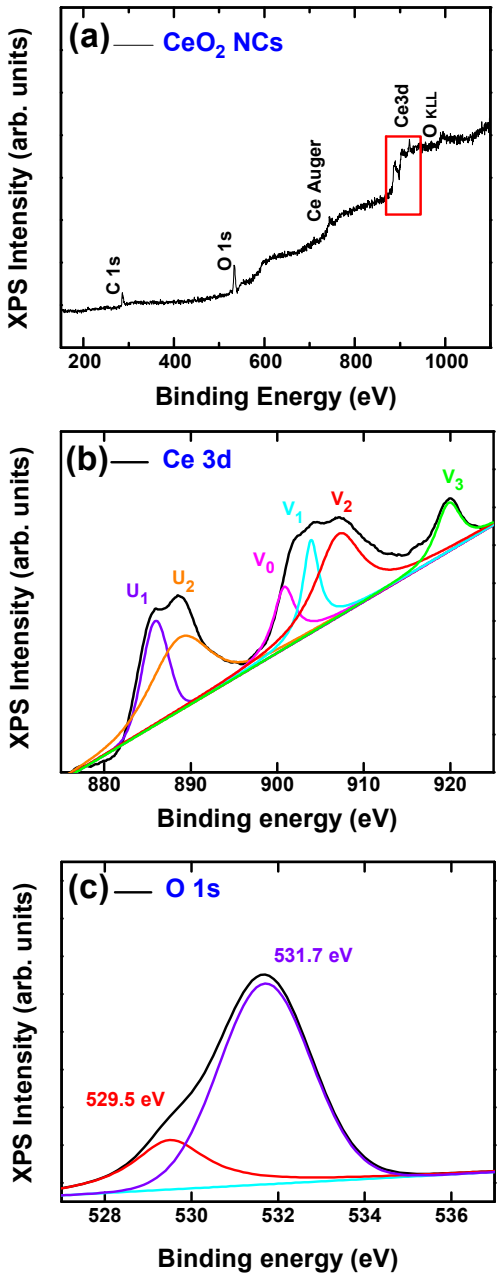

Fig. 3 (a) XPS survey spectrum of CeO_2 nanocrystals; core level spectra of (b) Ce 3d and (c) O 1s.

Fig. 1(d) illustrates the unit cell (1×1×1) of CeO_2 structure modeled through the Visualization for Electronic and Structural Analysis (VESTA) V3.2.1.[41,42] The CeO_2 crystals have a fluorite-type cubic structure with a space group ($Fm\bar{3}m$) and point-group symmetry (O_h). Moreover, cerium (Ce) atoms (lattice formers) are bonded to eight oxygen (O) atoms which form cube related to regular hexahedron [CeO_8] clusters.

Fig. 2(a-c) shows the TEM images of CeO_2 NCs with an average diameter of 10 nm. Fig. 2(d) displays a high resolution TEM (HR-TEM) image with an interplanar spacing distance of 0.311 nm corresponds to (111) plane of fluorite-type cubic structure of CeO_2 crystal,[18] which is consistent with the XRD and Rietveld refinement results. Besides, Fig. 2(e) displays the elemental composition of the CeO_2 NCs, which is found to be 72.15 wt% of Ce Lα, 16.81 wt% of O Kα and 11.04 wt% of C Kα (Carbon). The EDAX results confirm the presence of CeO_2 in the synthesized CeO_2 NCs.

To further confirm the composition and the chemical states of the samples, XPS analysis were performed. Fig. 3a displays the XPS survey spectrum of CeO_2 NCs and only Ce, C and O signals were observed on the surface of the CeO_2 NCs indicating the high purity of the sample. The C 1s peak is assigned to the adventitious carbon. Fig. 3b shows the Ce 3d core level XPS spectra of CeO_2 NCs, which can be deconvolved into six peaks. The peaks labeled as U_1, V_O, and V_1 are the characteristic peaks of Ce^{3+} states while U_2, V_2, and V_3 are the characteristic peaks of Ce^{4+} states.[43,44] The results indicate the co-existence of Ce^{3+} and Ce^{4+} states in CeO_2 NCs, which is consistent with the reported literatures.[45,46] Fig. 3c shows the O 1s core level XPS spectrum of CeO_2 NCs, which can be deconvolved into two peaks. The peak located at 529.5 eV is attributed to the oxygen bond of Ce-O-Ce, and the other peak centered at 531.7 eV corresponds to Ce-O-H, respectively.[47,48]

Fig. 4a shows the cyclic voltammogram (CV) of CeO_2 modified electrode in 0.1 M PBS solution at pH = 7 with a scan rate of 30 mV/s in the potential range of -0.4V to +0.6V. A well-defined redox peaks are observed at 0.24V and 0.1V respectively. It is observed that, the anodic peak current (i_{pa}) and cathodic peak current (i_{pc}) are almost equal (i_{pc}/i_{pa}=1.25). Fig. 4a shows the cyclic voltammogram (CV) of CeO_2 modified electrode in 0.1 M PBS solution at pH = 7 with a scan rate of 30 mV/s in the potential range of -0.4V to +0.6V. A well-defined redox peaks are observed at 0.24V and 0.1V, respectively. It is observed that, the anodic peak current (i_{pa}) and cathodic peak current (i_{pc}) are almost equal (i_{pc}/i_{pa}=1.25). Moreover, the redox peak potential difference (ΔE_p) is found to be 140 mV. For ΔE_p< 200 mV, the apparent rate constant (k^o) can be calculated using the Laviron's equation given by eq. (3),[49]

$$k^o = \alpha n F v/RT \quad (3)$$

where α is the transfer coefficient (0.5), n is number of electrons per molecule involved in electrochemical reaction (here, n=1), F is faradays constant, v is the scan rate, R is the gas constant, T is temperature. The calculated apparent rate constant value (k^o) is found to be 6.149 $x10^{-1}$ cm/s indicating the electrochemical reaction is quasi-reversible, which is consistent with the reported literature.[50] The CV curves of CeO_2 NCs modified electrode at various scan rates are displayed in Fig. 4b. As it is seen, both the anodic (i_{pa}) and cathodic (i_{pc}) peak currents are increased identically with increasing scan rates. Besides, there is a slight shift in the peaks with increase in scan rate.

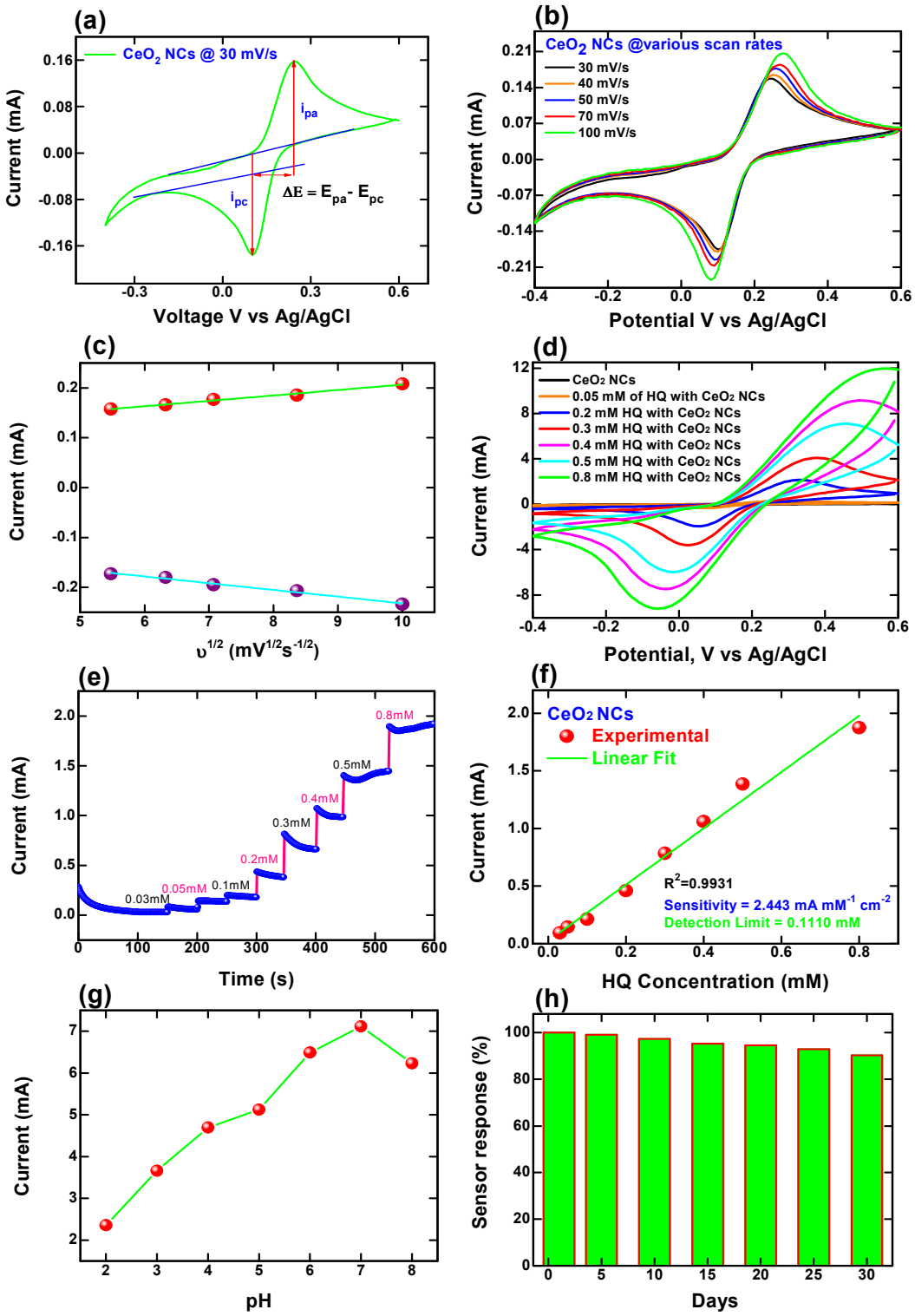

Fig. 4 (a) CV curve of CeO_2 nanocrystals at 30 mV/s in 0.1M PBS (b) CV curve of CeO_2 nanocrystals at various scan rates (c) Variation of peak current with square root of scan rates (d) CV curves at different HQ concentrations at 100 mV s^{-1} (e) Amperometric response (f) Calibration curve (g) Plot of oxidation peak current Vs pH at a scan rate of 100 mV s^{-1} in 0.5 mM HQ (h) Stability curve of CeO_2 nanocrystals modified electrode (pH 7).

Notably, the peak currents i_{pa} and i_{pc} are almost equal for all scan rates. The variation of i_{pa} and i_{pc} with square root of various scan rates are displayed in Fig. 4(c). The peak current is a linearly proportional to square root of scan rates which indicate the electrochemical process are diffusion controlled.[14]

The linear regression equations are E_{pa}= 0.0108 $v^{1/2}$ + 0.0981 (R=0.9935) and E_{pc}= -0.0134 $v^{1/2}$ - 0.0972 (R=0.99) in the linear range from 30 to 100 mV/s. The diffusion co-efficient (D) could be calculated using Randles-Sevcik equation given by eq. (4),

$$i_p = 2.69 \times 10^5 n^{3/2} A C D^{1/2} v^{1/2} \quad (4)$$

where i_p is the peak current, n is number of electrons per molecule involved in electrochemical reaction (here, n=1), A is area of the electrode, C is the bulk concentration, v is the scan rate (30 mV s^{-1}). The value of diffusion co-efficient (D) is calculated to be 1.1839 x 10^{-15} cm^2 s^{-1}.[51]

Moreover, the electrocatalytic oxidation of HQ by CeO_2 NCs is investigated through cyclic voltammetry. The CV curves of CeO_2 NCs with increasing concentration of HQ at a scan rate of 100 mV s^{-1} are given in Fig. 4(d). It is clearly evident that, there is an increase in peak current upon addition of HQ into the PBS solution from 0.05 mM to 0.8 mM. Scheme 1 shows the proposed reaction mechanism for the detection of HQ by using CeO_2 nanocrystals modified electrode. The oxygen species (O^-) supported in the oxidation of the HQ in to 1,4-benzoquinone and emits two free electrons and the CeO_2 NCs in the surface accepts the released electrons, resulting in the enhanced sensitivity towards HQ.[52] The increase in current about ~11 times is observed due to the addition of various HQ concentrations and this behaviour shows the good electrochemical sensing activity of prepared CeO_2 NCs.

The amperometric response of CeO_2 NCs modified electrode is shown in Fig. 4(e). The current of CeO_2 NCs increased gradually upon increasing HQ concentration. This amperometric response shows the stable and efficient electrocatalytic activity of CeO_2 NCs modified electrode. The calibration curve of CeO_2 NCs modified electrode is shown in Fig. 4(f), exhibits a linear increase in current with increase in HQ concentration.

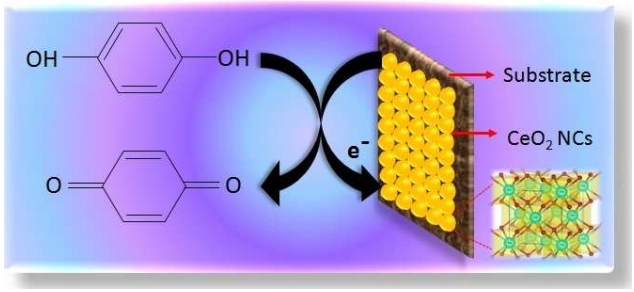

Scheme 1. A proposed reaction mechanism for the detection of hydroquinone by CeO_2 nanocrystals modified electrode.

The linear regression equation is I_p = 0.02439 + 2.44372C with a statistically significant correlation co-efficient of 0.9931(R^2) where peak current (Ip) is in mA and concentration (C) in mM. The sensitivity is estimated from the slope of the calibration curve and it is found to be 2.443 mA mM^{-1} cm^{-2}. As well, the minimum detection limit (LOD) is calculated using the eq. (5),[53]

$$\text{Limit of detection (LOD)} = 3S_b/q \quad (5)$$

where S_b is the standard deviation of the blank signal, and q is the slope of the calibration curve. The calculated minimum detection limit is found to be 0.111 mM.

The effect of pH on the electrocatalytic oxidation of HQ is studied in the pH range from 2 to 7 at a scan rate of 100 mV s^{-1} in the buffer solution containing 0.5 mM HQ. The peak current of CeO_2 NCs is increased with increase in pH and revealed a maximum current at pH 7 (Fig. 4g). After pH 7, the peak current is found to decreased.[12] Thus, pH 7 was chosen as the optimal value due to its high sensitivity.

Nevertheless, the long-term stability of the sensing systems is most essential for the real world consideration. In order to identify the stability of CeO_2 NCs modified electrode towards HQ sensing, the modified electrode was stored in PBS solution at room temperature and the sensitivity towards HQ is measured, as shown in Fig. 4(h). From the results, it is clear that the CeO_2 NCs modified electrode exhibits an excellent stability with less than 10% decrease from its initial sensitivity to final sensing process.

Conclusions

In summary, CeO_2 NCs were synthesized successfully by the precipitation method and we have investigated its electrochemical detection of HQ. XRD, Rietveld refinement data and TEM image analyses confirmed the presence of fluorite-type cubic structure of our CeO_2 NCs which is consistent with (ICSD) N°. 156250. HQ sensing of CeO_2 NCs/carbon paper (CP) modified electrode was characterized using a cyclic voltammetry (CV). The electrochemical sensing analysis of the modified electrode showed a detection limit of 0.111 mM and the linear ranges (0.03-0.8 mM) with a sensitivity of 2.443 mA mM^{-1} cm^{-2} for HQ detection. Our results showed that the CeO_2 NCs modified electrode holds as a promising candidate for the electrochemical detection of xenobiotic micro-pollutant HQ.

Acknowledgements

This work was supported by the Technology Innovation Program (10041957, Design and Development of fibre-based flexible display) funded by the Ministry of Trade, industry & Energy (MI, Korea). The Brazilian author acknowledges the financial support of agencies: CNPq (304531/2013-8), CAPES and FAPEPI.

Notes and references

1 Y. Zhang, G. M Zeng, L. Tang, D. L. Huang, X. Y. Jiang and Y. N. Chen, *Biosens. Bioelectron*., 2007, **22**, 2121-2126.
2 A. L. Jr. Buikema, M. J. Mc Ginniss and J. Jr. Cairns, *Mar. Environ. Res*., 1979, **2**, 87-181.
3 I. Buttino, M. Flippi and N. Cardellicchio, *Acqua Aria*, 1991, **9**, 853-861.
4 H. Cui, C. He and G. Zhao, *J. Chromatogr. A*, 1999, **855**, 171-179.
5 J. S. O. Grodnick, G .D. Dupre, B. J. Gulizia and S. H. Blake, *J. Chromatogr. Sci.*, 1983, **21**, 289-292.
6 L. Zhao, B. Lv, H. Yuan, Z. Zhou and D. Xiao, *Sensors*, 2007, **7**, 578-588.

7 M. F. Pistonesi, M. S. D. Nezio, M. E. Centurion, M. E. Palomeque, A. G. Lista and B. S. F. Band, *Talanta*, 2006, **69**, 1265-1268.
8 Y. Zhang, R. Sun, B. Luo and L. Wang, *Electrochim. Acta*, 2015, **156**, 228-234.
9 T. Y. Huang, C. W. Kung, H. Y. Wei, K. M. Boopathi, C. W. Chu and K. C. Ho, *J. Mater. Chem. A*, 2014, **2**, 7229-7237.
10 A. T. E. Vilian, S. M. Chen, L. H. Huang, M. Ajmal Ali and F. M. A. Al-Hemaid, *Electrochim. Acta*, 2014, **125**, 503-509.
11 L. Zaijun, S. Xiulan, X. Qianfang, L. Ruiyi, F. Yinjun, Y. Shuping and L. Junkang, *Electrochim. Acta*, 2012, **85**, 42-48.
12 T. Gan, J. Sun, K. Huang, L. Song and Y. Li, *Sensors Actuat B*, 2013, **177**, 412-418.
13 S. Radhakrishnan, K. Krishnamoorthy, C. Sekar, J. Wilson and S. J. Kim, *Chem. Eng. J.*, 2015, **259**, 594-602.
14 Y. H. Huang, J. H. Chen, X. Sun, Z. B. Su, H. T. Xing, S. R. Hu, W. Weng, H. X. Guo, W. B. Wu and Y. S. He, *Sens. Actuat. B*, 2015, **212**, 165-173.
15 Y. Zhang, S. Xiao, J. Xie, Z. Yang, P. Pang and Y. Gao, *Sens. Actuat. B*, 2014, **204**, 102-108.
16 K. J. Huang, L. Wang, Y. J Liu, T. Gan, Y. M. Liu, L. L. Wang and Y. Fan, *Electrochim. Acta*, 2013, **107**, 379-387.
17 M. U. A. Prathap, B. Satpati and R. Srivastava, *Sens. Actuat. B*, 2013, **186**, 67-77.
18 M. Melchionna, P. Fornasiero, *Mater. Today,* 2014, **17**, 349-357.
19 A. Trovarelli and P. Fornasiero, Catalysis by Ceria and Related Materials, Second Edition, *Imperial College Press*, 2002, London.
20 N. S. Arul, D. Mangalaraj and T. W. Kim, *Appl. Phys. Lett.*, 2013, **102**, 223115-1- 223115-4.
21 R. X. Valenzuela, G. Bueno, A. Solbes, F. Sapina, E. Martinez and V. C. Corberan, *Top. Catal*., 2001, **15**, 181-188.
22 T. S. Stefanik and H. L. Tuller, *J. Eur. Ceram. Soc*., 2001, **21**, 1967-1970.
23 C. W Sun, H. Li and L. Q. Chen, *Energy Environ Sci*., 2012, **5**, 8475-505.
24 A. Corma, P. Atienzar, H. Garcia and J. Y. C. Ching, *Nat. Mater*., 2004, **3**, 394-397.
25 X. Lu, D. Zheng, P. Zhang, C. Liang, P. Liu and Y. Tong, *Chem. Commun*., 2010, **46**, 7721-7723.
26 Y. Qiu, E. Rojas, R. A. Murray, J. Irigoyen, D. Gregurec, P. C. Hartmann, J. Fledderman, I. E. Lopis, E. Donath and S. E. Moya, *Nanoscale*, 2015, **7**, 6588-6598.
27 L. Han, R. Liu, C. Li, H. Li, C. Li, G. Zhang and J. Yao*, J. Mater. Chem*., 2012, **22**, 17079-17085.
28 S. K. Jha, C. N. Kumar, R. P. Raj, N. S. Jha, and S. Mohan, *Electrochim. Acta*, 2014, **120**, 308-313.
29 X. Zhao, Y. Du, W. Ye, D. Lu, X. Xia and C. Wang, *New J. Chem*., 2013, **37**, 4045-4051.
30 X. Jiao, H. Song, H. Zhao, W. Bai, L. Zhang and Y. Lv, *Anal. Methods*, 2012, **4**, 3261-3267.
31 F. Zhang, Q. Jin and S. W. Chan, *J. Appl. Phys.,* 2004, **95**, 4319-4326.
32 B. L. Cushing, V. L. Kolesnichenko and C. L. O. Connor, *J. Chem. Rev*., 2004, **104**, 3893-3946.
33 A. C. Cabral, L. S. Cavalcante, R. C. Deus, E. Longo, A. Z. Simoes and F. Moura, *Ceram. Internat*., 2014, **40**, 4445-4453.
34 S. W. Lee, D. Kim, H. J. Won and W. Y. Chung, *Electr. Mater. Lett*., 2006, **2**, 53-58.
35 H. M. Rietveld, *J. Appl. Cryst*., 1967, **22**, 151-152.
36 H. M. Rietveld, *J. Appl. Cryst.*, 1969, **2**, 65-71.
37 M. Bortolotti, L. Lutterotti and I. Lonardelli, *J. Appl. Cryst.*, 2009, **42**, 538-539.
38 A.R. Roosen, R.P. McCormack and W.C. Carter, *Comp. Mater. Sci.*, 1998, **11**, 16-26.
39 Y. L. Kuo, Y. M. Su and H. L. Chou, *Phys. Chem. Chem. Phys.,* 2015, 17, 14193-14200.
40 C. Suryanarayana, X-ray diffraction: a practical approach; Plenum Press: New York, 1998.
41 K. Momma and F. Izumi, *J. Appl. Crystallogr.*, 2008, **41**, 653-658.
42 K. Momma and F. Izumi, *J. Appl. Crystallogr.*, 2011, **44**, 1272-1276.
43 D. Jiang, W. Wang, E.Gao, S. Sun and L. Zhang, *Chem. Commun.,* 2014, **50**, 2005-2007.
44 F. Zhu, G. Chen, S. Sun and X. Sun, *J. Mater. Chem. A*, 2013, **1**, 288–294.
45 F. Meng, L. Wang and J. Cui, *J. Alloys Compd.*, 2013, **556**, 102-108.
46 S. Tsunekawa, J.T. Wang and Y. Kawazoe, *J. Alloys Compd*., 2006, **1145**, 408-412.
47 A. Galtayries, R. Sporken, J. Riga, G. Blanchard and R.Caudano, *J. Electron. Spectrosc. Relat. Phenom*., 1998, **88-91**, 951-956.
48 L. T. Murciano, A. Gilbank, B. Puertolas, T. Garcia, B. Solsona and D. Chadwick, *Appl. Catal., B Environ*., 2013, **132-133**, 116-122.
49 E. Laviron, *J. Electroanal. Chem*., 1979, **101**, 19-28.
50 J. Wang, Analytical Electrochemistry, Second Edition, 2000 Wiley-VCH.
51 W. Yuan, Y. Zhou, Y. Li, C. Li, H. Peng, J. Zhang, Z. Liu, L. Dai and G. Shi, *Sci. Rep*., 2013, **3**, 2248-7.
52 G. N. Dar, A. Umar, S. A. Zaidi, A. A. Ibrahimd, M. Abaker, S. Baskoutas, M. S. Al-Assiri, *Sens. Actuat. B*, 2012, **173**, 72-78.
53 J. Mocak, A. M. Bond, S. Mitchell and G. Scollary, *Pure Appl. Chem*., 1997, **69**, 297-328.